HHS Public Access

Author manuscript

Sci Signal. Author manuscript; available in PMC 2018 October 24.

Published in final edited form as:

Sci Signal. ; 11(527): . doi:10.1126/scisignal.aaq1616.

A defect in KCa3.1 channel activity limits the ability of CD8+ T cells from cancer patients to infiltrate an adenosine-rich microenvironment*

Ameet A. Chimote[1], **Andras Balajthy**[1,†], **Michael J. Arnold**[1], **Hannah S. Newton**[1], **Peter Hajdu**[1,‡], **Julianne Qualtieri**[2], **Trisha Wise-Draper**[3], and **Laura Conforti**[1,†]

[1]Department of Internal Medicine, Division of Nephrology, University of Cincinnati, Cincinnati, Ohio, 45267, USA

[2]Department of Pathology, University of Cincinnati, Cincinnati, Ohio, 45267, USA

[3]Department of Internal Medicine, Division of Hematology-Oncology, University of Cincinnati, Cincinnati, Ohio, 45267, USA

Abstract

The limited ability of cytotoxic T cells to infiltrate solid tumors hampers immune surveillance and the efficacy of immunotherapies in cancer. Adenosine accumulates in solid tumors and inhibits tumor-specific T cells. Adenosine inhibits T cell motility through the A_{2A} receptor ($A_{2A}R$) and suppression of KCa3.1 channels. Herein, we conducted 3-dimensional chemotaxis experiments to elucidate the effect of adenosine on the migration of peripheral blood $CD8^+$ T cells from head and neck squamous cell carcinoma (HNSCC) patients. The chemotaxis of HNSCC $CD8^+$ T cells was reduced in the presence of adenosine, and the effect was greater on HNSCC $CD8^+$ T cells than on healthy donor (HD) $CD8^+$ T cells. This response correlated with the inability of $CD8^+$ T cells to infiltrate tumors. The effect of adenosine was mimicked by an $A_{2A}R$ agonist and prevented by an $A_{2A}R$ antagonist. We found no differences in $A_{2A}R$ expression, cAMP abundance, or protein kinase A1 activity between HNSCC and HD $CD8^+$ T cells. We instead detected a decrease in KCa3.1 channel activity, but not expression, in HNSCC $CD8^+$ T cells. Activation of KCa3.1 channels by 1-EBIO restored the ability of HNSCC $CD8^+$ T cells to chemotax in the presence of adenosine. Our data highlight the mechanism underlying the increased sensitivity of HNSCC

---

†To whom correspondence should be addressed: Laura Conforti, Department of Internal Medicine, Division of Nephrology, University of Cincinnati, 231 Albert Sabin Way, Cincinnati, OH 45267-0585; laura.conforti@uc.edu.
†Current address: Department of Pediatrics, Faculty of Medicine, University of Debrecen, Egyetem tér 1., Debrecen, 4032, Hungary.
‡Current address: Department of Biophysics and Cell Biology, Faculty of Dentistry, University of Debrecen, Egyetem tér 1., Debrecen, 4032, Hungary.

Author contributions: Conception and design: AAC, AB, LC, Development of methodology: AAC, LC, AB, MJA, HSN, Acquisition of data: AAC, AB, MJA, HSN, PH, JQ, Provided and managed patients: TW-D. Provided patient data: TW-D, JQ, Analysis and interpretation of data: AAC, AB, MJA, HSN, PH, JQ TW-D and LC, Writing, review, and/or revision of the manuscript: AAC, LC, Study supervision: LC. All authors discussed the results and commented on the manuscript.

Competing interests: The authors declare that they have no competing interests.

Data and materials availability: All data needed to evaluate the conclusions in the paper are present in the paper or the Supplementary Materials.

$CD8^+$ T cells to adenosine and the potential therapeutic benefit of KCa3.1 channel activators, which could increase infiltration of these T cells into tumors.

Introduction

The immune system plays an important role in cancer. In many solid malignancies, including head and neck squamous cell carcinoma (HNSCC), an increased infiltration of cytotoxic $CD8^+$ T cells into the tumor mass is often associated with good prognosis and response to therapy (1–3). This knowledge is indeed at the foundation of immune therapies that increase the number and functionality of cytotoxic tumor-infiltrating lymphocytes (TILs). Adoptive T cell (ATC) transfer, chimeric antigen receptor (CAR) T cells, and checkpoint inhibitors have shown promising results in many forms of cancer. Whereas these therapies are very effective in increasing the functional capabilities of T cells, the modified T cells still maintain a limited ability to infiltrate the tumor mass and resist the immunosuppressive tumor microenvironment (TME) (4–7). The inability of tumor-specific T cells to traffic to a solid tumor represents a great challenge for effective immunotherapy. The unique features of the TME contribute to the reduced infiltration and functionality of TILs (8). Thus, understanding how the TME limits T cell infiltration is necessary for improving immune surveillance in cancer and developing effective immunotherapies.

The purine nucleoside adenosine accumulates in the TME, and has been associated with tumor progression, enhanced metastatic potential, and poor prognosis (9–11). In vivo studies provide conclusive evidence of the importance of adenosine in cancer (12–15). Abrogation of the adenosine signaling pathway, either through knockdown of the A_{2A} adenosine receptor ($A_{2A}R$), a G-protein coupled receptor (GPCR) expressed in immune cells, or by $A_{2A}R$ antagonists, reduces tumor burden in tumor-bearing mice, increases survival, and increases the efficacy of immunotherapies (5, 6, 9, 16–18). Furthermore, knockdown of CD73, an enzyme necessary for adenosine production, completely restores the efficacy of ATC therapies and leads to long-term tumor-free survival of tumor-bearing mice (19, 20). Adenosine is thus emerging as an important checkpoint inhibitor of the anti-tumor T cell response (21). Additionally, we have shown that adenosine limits cytokine release and motility in human peripheral blood T lymphocytes through calcium-activated KCa3.1 potassium channels (22).

Ion channels regulate multiple functions of T lymphocytes including cytokine, granzyme B production, and motility (23–26). Two K^+ channels, the voltage-dependent Kv1.3 and the Ca^{2+}-activated KCa3.1, regulate the electrochemical driving force for Ca^{2+} influx that is necessary for NFAT (nuclear factor of activated T cells) nuclear translocation, gene expression, and effector functions (26). These two channels also mediate the response to two key immune suppressive elements of the TME: hypoxia (Kv1.3) and adenosine (KCa3.1) (22, 27–29). Defects in Kv1.3 channels have been reported in TILs and are associated with their diminished cytotoxicity (30). The importance of K^+ channels of T lymphocytes in cancer was confirmed in mice where overexpression of the Kv1.3 channel increased interferon-γ (IFN-γ) production, reduced tumor burden, and increased survival (31, 32). We have shown that in human T lymphocytes, KCa3.1 channels reside at the uropod of polarized

mobile T cells and mediate the inhibitory effect of adenosine (22, 24). Adenosine, through $A_{2A}R$, stimulates cAMP production and protein kinase A1 (PKAI) activation, inhibits KCa3.1 channels, and suppresses T cell motility (22). We speculated that this mechanism could have important implications in the ability of effector T cells to infiltrate the tumor mass. Furthermore, it may be particularly important in HNSCC, where effector T cells are more sensitive to adenosine than are their healthy counterparts; that is, adenosine inhibits proliferation and cytokine release more in HNSCC effector T cells than in healthy donor cells (HD) (33). This enhanced sensitivity has been attributed to a reduction in adenosine deaminase activity and increased $A_{2A}R$ signaling. To date, the chemotactic abilities of HNSCC $CD8^+$ T cells and their response to adenosine have not been studied. In the present study, we investigated the effect of adenosine on the chemotaxis of circulating $CD8^+$ T cells of HNSCC patients and the mechanisms that mediate their heightened response to adenosine. We provide evidence of a role for KCa3.1 channels in the adenosine-mediated suppression of the chemotaxis of HNSCC $CD8^+$ T cells and suggest KCa3.1 channels may have therapeutic potential to increase the ability of HNSCC $CD8^+$ T cells to infiltrate an adenosine-rich TME.

Results

The chemotaxis of circulating $CD8^+$ T cells of HNSCC patients is impaired by adenosine

The TME is characterized by rapidly dividing tumor cells in a fibrous matrix with a variable degree of immune cell infiltrate. Adenosine accumulates in the hypoxic TME and the increased adenosine concentration contributes to the inhibition of the anti-tumor immune response by cytotoxic $CD8^+$ T cells (10, 34). Experiments were performed to assess whether adenosine had any effect on the chemotaxis of HNSCC $CD8^+$ T cells (for the demographic and clinicopathologic features of the patients see Table 1 and Table S1, respectively). We studied the effect of adenosine on the chemotaxis of activated HNSCC $CD8^+$ T cells in a tumor-like experimental setting and compared it to that of $CD8^+$ T cells from healthy donors (HDs). To mimic the TME, we used the μ-Slide chemotaxis chamber, which enables the generation of a stable, three-dimensional collagenous matrix in which $CD8^+$ T cells migrate in response to a chemokine gradient (35, 36). All chemotaxis experiments were conducted with CXCL12 (37). Also, all experiments were conducted on $CD8^+$ T cells activated in vitro with anti-CD3 and anti-CD28 antibodies for 3–4 days, unless otherwise specified. In the absence of CXCL12, cells exhibited random migration within the collagen matrix, whereas in the presence of a CXCL12 gradient, the cells migrated towards the highest CXCL12 concentration (Fig. S1 and Fig. 1A–B, Table S2). We observed no significant differences in the baseline chemotactic response of HD and HNSCC $CD8^+$ T cells as indicated by similar values for Y-COM (Y coordinate of the Center of Mass, i.e. the averaged position the cells achieved at the end of the experiment; red triangles in Fig. 1 and S1), FMI^Y (Y coordinate of the Forward Migration Index), velocity, accumulated distance, directness and Euclidean distance (Table S2). Hereafter, Y-COM is used to quantify a chemotactic response. To evaluate what effect adenosine had on the chemotaxis of HD and HNSCC $CD8^+$ T cells, we measured CXCL12-driven chemotaxis in the presence or absence of a concomitant adenosine gradient. Adenosine inhibited chemotaxis and this effect was significantly more pronounced in HNSCC $CD8^+$ T cells than in HD T cells (Fig. 1, A and B). Adenosine

decreased Y-COM in cells from 5 out of 7 HDs (Fig. 1 C). In contrast, HNSCC $CD8^+$ T cells displayed greater sensitivity to adenosine than did their healthy counterparts (Figure 1D). Activated T cells from HDs exhibited an 26% overall reduction in the Y-COM values, whereas adenosine inhibited the Y-COM values of HNSCC donor cells by 80% (Fig 1E). Overall, HNSCC cells lost their chemotactic ability in the presence of adenosine, as indicated by loss of significant differences between Y-COM and X-COM values (the COM Y and X coordinates), and between FMI^y and FMI^x (FMI in the X and Y directions; Fig. 1B, Table 2). Note that adenosine did not induce any significant changes in other parameters that define T cell migration, such as cell velocity, directness, or accumulated distance in either HD or HNSCC $CD8^+$ T cells (Table 2). Overall, these data show that adenosine inhibits the chemotaxis of HNSCC $CD8^+$ T cells. To test if adenosine accumulation might explain the inability of $CD8^+$ T cells to infiltrate the adenosine-rich TME, we performed immunohistochemical staining of HNSCC tumors for CD8 and CD73 (ecto-5′-nucleotidase), an enzyme responsible for adenosine production that is used as a marker of adenosine abundance in solid tumors (19). We found a mixed degree of $CD8^+$ infiltration and CD73 expression in HNSCC tumors (Fig. 2A–B, Table S1). However, in the small cohort of patients with high intratumoral CD73 expression (n=9), there was a negative correlation between the effect of adenosine on chemotaxis in vitro and $CD8^+$ T cell tumor infiltration, i.e. the patients whose $CD8^+$ T cells chemotaxis was most inhibited by adenosine were also those that had the lowest $CD8^+$ T cell infiltration into the tumor (Fig. 2C; Table S1).

The $A_{2A}R$ mediates the suppressive effect of adenosine on the chemotaxis of HNSCC $CD8^+$ T cells

We conducted experiments to define whether the $A_{2A}R$ mediates the inhibitory effect of adenosine on HNSCC $CD8^+$ T cells. The selective $A_{2A}R$ agonist CGS21680 suppressed the chemotaxis of HNSCC $CD8^+$ T cells in a way comparable to adenosine (Fig. 3A–B) (22, 38). We observed that the Y-COM of HNSCC $CD8^+$ T cells was reduced by CGS21680 (Fig 3A). In 4 of these 6 patients, we simultaneously tested the effect of adenosine, and the Y-COM was not significantly different from that in the presence of CGS21680 (Fig. 3A). Overall, the degree of Y-COM reduction was similar in the presence of CGS21680 and adenosine (Fig. 3B). The involvement of the $A_{2A}R$ was further confirmed with SCH58261, a selective $A_{2A}R$ competitive antagonist (22). The inhibitory effect of adenosine on HNSCC $CD8^+$ T cells was abrogated when the cells were pre-treated with SCH58261 (Fig. 3C). The cells pre-treated with SCH58261 still migrated towards CXCL12 even in the presence of adenosine, as shown by the increased Y-COM values when compared to cells not treated with SCH58621 (Fig. 3C). The adenosine-induced reduction in the Y-COM value of HNSCC $CD8^+$ T cell chemotaxis was blocked by SCH58261 (Fig. 3D). Overall, we showed that the adenosine-mediated inhibition of chemotaxis of HNSCC $CD8^+$ T cells occurs through the $A_{2A}R$. These data suggest that blockade of the $A_{2A}R$ could increase the ability of circulating $CD8^+$ T cells of HNSCC patients to migrate towards a chemokine.

$A_{2A}R$ expression and cAMP-PKA signaling are not altered in HNSCC $CD8^+$ T cells

The $A_{2A}R$ signals through the activation of adenylate cyclase and, in turn, induces an increase in cAMP, PKAI activation, and inhibition of KCa3.1 channels (11, 22).

Experiments were performed to assess whether alterations in components of the adenosine signaling pathway mediate the inhibitory effect of adenosine on the chemotaxis of HNSCC $CD8^+$ T cells. Increased $A_{2A}R$ abundance, increased cAMP- PKAI signaling, or decreased KCa3.1 activity in HNSCC $CD8^+$ T cells could explain their enhanced sensitivity to adenosine. We measured *ADORA2A* expression (Fig. 4A) as well as $A_{2A}R$ protein abundance (Fig. 4B–D) in $CD8^+$ T cells in HDs and HNSCC patients and found no significant differences in either mRNA or protein expression. We further investigated if there were any differences in the signaling pathway downstream of the $A_{2A}R$. We did not observe any significant difference in the intracellular cAMP concentrations in activated HD and HNSCC $CD8^+$ T cells (Fig. 4E). Similarly, we could not detect statistically significant differences in PKA activity following $A_{2A}R$ stimulation between HD and HNSCC $CD8^+$ T cells (Fig. 4F). Overall, our results show that decreased migration of HNSCC $CD8^+$ T cells in the presence of adenosine was not due to any differences in $A_{2A}R$ abundance or proximal signaling.

KCa3.1 channel activity is reduced in HNSCC $CD8^+$ T cells

KCa3.1 channels are downstream of PKA in the adenosine signaling pathway, and we have previously shown that adenosine reduces T cell motility by inhibiting KCa3.1 channels (22). Hence, we conducted experiments to measure whether alterations in KCa3.1 channels in HNSCC $CD8^+$ T cells could explain the adenosine-dependent inhibition of chemotaxis. KCa3.1 channels are present at the uropod of migrating T cells and mediate their migration (24). KCa3.1 channels are also involved in the chemotaxis of HD and HNSCC $CD8^+$ T cells because the KCa3.1-specific blocker TRAM-34 inhibited their migration (Fig. S2) (39). We thus evaluated the expression and function of KCa3.1 channels in resting and activated HNSCC $CD8^+$ T cells and compared them to those of HD $CD8^+$ T cells (Fig. 5). KCa3.1 channel expression in T lymphocytes increases with activation (40). Patch-clamp experiments showed that the KCa3.1 activity (defined by the whole-cell KCa3.1 conductance normalized to the cell membrane capacitance) was significantly lower in activated HNSCC $CD8^+$ T cells as compared to their HD counterparts (Fig. 5A–B, Table S3). No differences were observed in resting HD or HNSCC $CD8^+$ T cells (Table S3). There were no changes in the Kv1.3 activity (reported here as current density: peak current/ capacitance) in either resting or activated HD or HNSCC $CD8^+$ T cells (Fig. 5C, Table S3). The data were normalized for the capacitance as there was a significant difference in cell capacitance between activated, but not resting, HD and HNSCC $CD8^+$ T cells (Table S3). Because activation increased KCa3.1 channel expression and capacitance, which is a measure of the cell size, these data raise the possibility that HNSCC $CD8^+$ T cells are less activated than HD $CD8^+$ T cells. We thus measured KCa3.1 expression by flow cytometry in resting and activated $CD8^+$ T cells in HD and HNSCC patients and observed that upon activation, KCa3.1 channel abundance was similarly increased in both HD and HNSCC $CD8^+$ T cells (Fig. 5D–E). In both HD and HNSCC $CD8^+$ T cells, there were comparable increases in the mean fluorescence intensity (MFI) of KCa3.1 after activation (Fig. 5F). We also measured CD69 abundance as marker of activation and observed no statistically significant difference between HNSCC and HD $CD8^+$ T cells (Fig. S3). This suggests that the decreased KCa3.1 channel activity in HNSCC $CD8^+$ T cells is not likely due to a

decrease in channel surface expression or defective T cell activation. Overall, these data show that there is reduced KCa3.1 activity, but not expression, in HNSCC $CD8^+$ T cells.

Activation of KCa3.1 restores the chemotaxis of HNSCC $CD8^+$ T cells in the presence of adenosine

Experiments were conducted to determine whether activation of KCa3.1 channels by 1-EBIO, a selective positive modulator of KCa3.1 channels, abolished the inhibitory effect of adenosine on the chemotaxis of HNSCC $CD8^+$ T cells (41). We evaluated whether increasing the activity of KCa3.1 channels with 1-EBIO would enable the HNSCC $CD8^+$ T cells to migrate towards a chemokine even in the presence of adenosine. 1-EBIO increased the activity of KCa3.1 channels in activated HNSCC $CD8^+$ T cells to a level comparable to that of the baseline conductance in HD $CD8^+$ T cells (without 1-EBIO) (Fig. 6A). Consistent with our earlier findings (Fig. 5A–B), KCa3.1 conductance in HNSCC $CD8^+$ T cells in the absence of 1-EBIO was also significantly lower than that in HD $CD8^+$ T cells. The Y-COM values of HNSCC $CD8^+$ T cells that underwent chemotaxis towards CXCL12 was significantly reduced in the presence of adenosine (Fig. 6B), similar to our earlier finding (Fig. 1). However, when HNSCC $CD8^+$ T cells from the same individuals were pre-incubated with 1-EBIO, the Y-COM values in the presence of adenosine were almost 3-fold greater than those of cells in the presence of adenosine without 1-EBIO. Thus, the inhibitory effect of adenosine on the chemotaxis of HNSCC $CD8^+$ T cells was blocked by 1-EBIO (Fig. 6C). A similar effect was caused by NS309, a more potent activator of KCa3.1 channels (42). Preincubation of $CD8^+$ T cells from two HSCC patients with NS309 reversed the inhibitory effect of adenosine on chemotaxis to CXCL12 (Fig. S4). These findings suggest that enhancing KCa3.1 function in HNSCC $CD8^+$ T cells restores their ability to chemotax in the presence of adenosine.

Discussion

The unequivocal prognostic and therapeutic significance of $CD8^+$ T cell infiltration in most solid tumors and the known immunosuppressive properties of adenosine have driven the studies reported herein. The data we present suggest that the chemotaxis of circulating HNSCC $CD8^+$ T cells may be compromised in an adenosine-rich microenvironment because these cells, contrary to their healthy counterparts, have reduced KCa3.1 channel activity. Furthermore, these data highlight the therapeutic potential of KCa3.1 activators to increase penetration of $CD8^+$ T cells into tumors by abrogating the inhibitory effect of adenosine on the chemotaxis of $CD8^+$ T cells.

The failure of immune surveillance in cancer has been attributed to the lack of effective MHC presentation by cancer cells and the immunosuppressive properties of the TME (8). Indeed, new immunotherapies have been designed to increase the functionality of T cells and their ability to resist the TME (6, 43, 44). A prerequisite for cytotoxic functionality is direct contact with tumor cells. To this effect, a high intratumoral $CD8^+$/Treg (regulatory T cells) ratio is associated with good prognosis and response to therapy in multiple solid malignancies, including HNSCC (45). Thus, infiltration of $CD8^+$ T cells is a limiting step in the efficacy of immune surveillance and immunotherapies in cancer. The TME is rich in the

immunosuppressant adenosine (10). We showed that adenosine inhibited $CD8^+$ T cell chemotaxis, and this effect was enhanced in cells from HNSCC patients. This is consistent with immunohistochemical data of various solid tumors showing an inverse correlation between CD73 in the tumor and the infiltration of $CD8^+$ TILs (46–50). The advantage of the studies we have performed here over the correlative studies in tissue samples is that we have used a collagen-rich 3D microenvironment where we have full control over the experimental conditions used, while in vivo, the TME is a complex mixture of metabolic and waste products and tumor cells. This 3D system enables us to exclusively study the effect of adenosine on chemotaxis. We found that adenosine inhibited chemotaxis of HNSCC $CD8^+$ T cells. The chemotaxis experiments reported herein showed that HNSCC $CD8^+$ T cells lost directionality in the presence of adenosine, but maintained their velocity and overall distance traveled. The effect of adenosine in 3D chemotaxis experiments does not fully recapitulate what we have previously observed in a 2D migration assay on ICAM-1 surfaces where adenosine inhibited integrin-mediated random migration of HD $CD3^+$ T cells by reducing their velocity (22). The different experimental conditions and signaling pathways triggered by the different migratory stimuli may explain these discrepancies.

We found that adenosine had a more substantial inhibitory effect on the migration of HNSCC $CD8^+$ T cells than HD $CD8^+$ T cells. The degree of chemotaxis inhibition by adenosine in HNSCC $CD8^+$ T cells negatively correlated with the number of $CD8^+$ TILs in CD73 positive tumors underscoring the importance of this effect on immune surveillance in cancer. This also raises the possibility that the chemotactic sensitivity to adenosine of circulating $CD8^+$ T cells could be used as a minimally invasive biomarker of $CD8^+$ TIL infiltration and, possibly, prognosis. Larger population studies are necessary to confirm this possibility.

The increased sensitivity to adenosine that we observed in HNSCC $CD8^+$ T cells is in agreement with the heightened suppression of cytokine production and proliferation of HNSCC $CD8^+$ T cells by adenosine reported previously by Mandapathil *et al.* (33). They attributed this increased sensitivity to the reduced ability of HNSCC effector T cells (T_{eff}) to degrade and internalize adenosine as well as an amplified $A_{2A}R$ signaling as compared to HDs' T_{eff} (33). We observed a comparable effect of adenosine and the $A_{2A}R$ agonist CGS21680 on the chemotaxis of HNSCC $CD8^+$ T cells, suggesting that differences in the adenosine signaling pathway and not adenosine degradation are responsible for the heightened effect of adenosine on chemotaxis. It is well established that $A_{2A}R$ mediates the effect of adenosine in human T cells (5, 17, 51–53). We have previously shown that adenosine inhibits the motility of human $CD3^+$ T cells and cytokine release through $A_{2A}R$ stimulation, activation of adenylyl cyclase and PKAI, and ultimately inhibition of KCa3.1 channels (22). Therefore, it is anticipated that an increase in $A_{2A}R$, cAMP, and PKAI in HNSCC $CD8^+$ T cells could amplify the response to adenosine. Similarly, a reduction in functional KCa3.1 channels could reduce the functionality of the cells once they are exposed to adenosine, but it could also contribute to the reduced ability of HNSCC T cells to produce IL-2 and IFNγ as compared to HDs' cells, which was previously reported (33). Our data indicated no significant differences in $A_{2A}R$ expression, cAMP abundance, or $A_{2A}R$-stimulated PKAI activation in HNSCC T cells. We instead detected a decrease in KCa3.1 activity. This was not due to reduced KCa3.1 expression. Activated HD and HNSCC $CD8^+$

T cells had similar amounts of KCa3.1 membrane proteins as determined by flow cytometry. Despite the low KCa3.1 whole-cell conductance, we observed no difference in baseline chemotaxis (in the absence of adenosine) between HNSCC and HD $CD8^+$ T cells. It appears that only a fraction of KCa3.1 channel activity may be sufficient to guarantee chemotaxis. Further single-channel electrophysiological studies as well as evaluation of the downstream signaling pathways are necessary to understand the mechanism by which KCa3.1 channels regulate chemotaxis in T cells.

The findings reported in this manuscript indicate that restoring KCa3.1 activity in HNSCC $CD8^+$ T cells by 1-EBIO and NS309 abrogated the inhibitory effect of adenosine. KCa3.1 are Ca^{2+} sensitive K^+ channels that open upon an increase in intracellular Ca^{2+} concentration. 1-EBIO is a positive modulator of KCa3.1 channels, which increases their Ca^{2+} sensitivity (41). Eil *et al.* showed that pharmacological activation of KCa3.1 channels by positive modulators such as 1-EBIO improved $CD8^+$ T cell function in vitro and may potentially be of therapeutic use in cancer (31). The data we presented suggest that KCa3.1 activators could have therapeutic benefit by restoring the chemotactic capacity of $CD8^+$ T cells in an adenosine-rich TME, which would favor tumor penetration. The effect of KCa3.1 activation was comparable to that obtained by $A_{2A}R$ blockade, which has already shown to be of clear benefit in combination with anti-PD1 antibody or CAR-T cells in pre-clinical models of solid malignancies (5, 6, 17). A therapy based on KCa3.1 activation would have advantages over $A_{2A}R$ inhibition. KCa3.1 channels are downstream of other GPCRs. Prostaglandin E2 (PGE2), which is also present in the TME, inhibits KCa3.1 channels in mast cells (54). Thus, activation of KCa3.1 channels could be a more effective approach for improving immune surveillance and the response to immune therapies in cancer as it could simultaneously counteract multiple immune suppressive components of the TME.

Materials and Methods

Human Subjects

Studies were conducted on peripheral blood obtained from 39 de-identified HNSCC patients in the age range of 34–77. The eligibility criteria for patient inclusion in the study were a positive diagnosis for HNSCC confirmed by tissue biopsy, and no administration of radiation or chemotherapy prior to the time of drawing the blood (see Table 1 for patient demographics and table S1 for clinical information). The data on the study subjects were collected and managed using REDCap electronic data capture tools hosted at the University of Cincinnati. Peripheral blood was also drawn from 20 age-matched (±5 years) healthy donors (HD, 8 female, 12 male) in the age range of 24–67 years. Discarded blood units from Hoxworth Blood Center (University of Cincinnati) were used for preliminary chemotaxis validation experiments as well as for the *ADORA2A* RT-qPCR and the 1-EBIO electrophysiological experiments. Informed consent was obtained from all HNSCC patients as well as HDs. The study and informed consent forms were approved by the University of Cincinnati Institutional Review Board (IRB # 2014–4755).

Reagents and chemicals

Human serum, L-glutamine, adenosine, SCH58261, 1-EBIO and sodium hydroxide were purchased from Sigma-Aldrich. HEPES, RPMI-1640, fetal bovine serum, penicillin, streptomycin, and phosphate-buffered saline were obtained from Gibco. Rat-tail collagen I was obtained from Corning Inc. CGS21680 hydrochloride and NS309 were purchased from Tocris Bioscience, whereas CXCL12 was obtained from R&D systems. TRAM-34 was a kind gift from Dr. Heike Wulff (Department of Pharmacology, University of California Davis). Stock solutions of SCH58261, CGS21680, TRAM-34, 1-EBIO and NS309 were prepared in dimethyl sulfoxide (DMSO) and used at 0.1% dilution. Stock solution of CXCL12 was prepared in sterile PBS containing 0.1% bovine serum albumin (BSA).

Cell isolation and activation

PBMCs were isolated from whole blood by Ficoll-Paque density gradient centrifugation (GE Healthcare Bio-sciences), as described previously (55). $CD8^+$ T cells were subsequently isolated from PBMCs by negative selection using the EasySep Human $CD8^+$ T Cell Enrichment Kit (STEMCELL Technologies Inc.) according to the manufacturer's instructions. The $CD8^+$ T cells were maintained in RPMI-1640 medium supplemented with 10% human serum, 200 u/ml penicillin, 200 μg/ml streptomycin, 1 mM L-glutamine, and 10 mM HEPES (55). Cells were activated for 72–96 h in a cell culture dish coated with 10 μg/ml mouse anti-human CD3 antibody (Biolegend) and 10 μg/ml mouse anti-human CD28 antibody (Biolegend).

RT-qPCR

Total RNA was isolated from activated HD and HNSCC $CD8^+$ T cells using the E.Z.N.A. total RNA isolation kit (Omega-Biotek) as per the manufacturer's instructions. Six hundred and fifty nanograms of RNA was used to synthesize cDNA using Maxima First Strand cDNA Synthesis Kit for RT-qPCR (ThermoFisher Scientific) as per the manufacturer's instructions. Predesigned primers for RT-qPCR were obtained using TaqMan Gene Expression Assays (Applied Biosystems, ThermoFisher Scientific) to detect the expression of *ADORA2A* (Assay ID: Hs001169123_m1) and *GAPDH* (Assay ID: HS03929097_g1). The RT-qPCR was set up in a 96-well plate by adding 30 ng of cDNA, 1× TaqMan Gene Expression Master Mix (Applied Biosystems), and 1 μl of TaqMan Gene Expression Assay primers. All samples were run in quadruplicate. *GAPDH* was used as an internal control. RT-qPCR was cycled in Applied Biosystems StepOne Real-time PCR system (Applied Biosystems). C_T values were measured using StepOne software version 2.1 (Applied Biosystems). C_T values for *ADORA2A* were normalized against measured C_T values for *GAPDH* and the $\Delta\Delta C_T$ values were calculated as described previously (56). Relative quantity values, representing the fold-change in *ADORA2A* gene expression in HNSCC $CD8^+$ T cells compared to HD $CD8^+$ T cells, were calculated as the $2^{-\Delta\Delta CT}$ values.

Flow cytometry

$CD8^+$ T cells (~1×10^6 cells per condition) were fixed with 4% paraformaldehyde (Affymetrix) and stained with ATTO-488 conjugated mouse anti-human KCa3.1 antibody (Clone 6C1, Alomone Labs). Cells were then permeabilized with 0.1% Triton-X 100

(Sigma-Aldrich) and stained Alexa Fluor 405 conjugated mouse anti-human $A_{2A}R$ antibody (Clone 2D1, Novus Biologicals). To test T cell activation, $CD8^+$ T cells were stained live with Alexa Flour 488 conjugated anti-CD69 antibody (Clone FN50, Biolegend) and fixed with 1% paraformaldehyde. Data were collected on a LSR II flow cytometer (BD Biosciences) and analyzed with FlowJo software (Flow Jo LLC).

Chemotaxis

Three-dimensional chemotaxis was performed using the μ-Slide Chemotaxis assay (ibidi GmbH) according to the manufacturer's instructions. Briefly, ~1×10^6 activated $CD8^+$ T cells were incorporated in a type I rat-tail collagen gel (Corning) and added to the central observation chamber of the μ-Slide Chemotaxis. In all experiments, CXCL12 (8 μg/ml) was added to the migration medium in the reservoir to the left of the observation chamber, while migration medium without chemokine was added to the reservoir to the right of the observation chamber, thus generating a chemokine gradient to measure the baseline chemotaxis. To assess the effects of adenosine or CGS21680 on chemotaxis, simultaneous adenosine (or CGS21680) and chemokine gradients were established in a separate chamber by injecting adenosine (10 μM) or CGS21680 (10 μM), and CXCL12 (8 μg/ml) into the left reservoir. The slide was mounted on the stage of an inverted Zeiss LSM 710 microscope (Carl Zeiss Microscopy GmbH) equipped with a 37°C incubator. Cell migration was recorded by time-lapse video microscopy, with brightfield images acquired every 3 seconds for up to 3 hours. Cell tracking on the time-lapse images was performed using the "Manual tracking plugin" on ImageJ software (National Institutes of Health) and the data were analyzed using the Chemotaxis and Migration Tool (ibidi GmbH). On average, 15–20 cells were tracked per condition. The following chemotactic parameters were derived: 1) center of mass (COM, the average position along the relevant axis the cells reached by the end of the experiment); 2) Euclidian distance (the linear distance between the starting point and ending point of a cell); 3) accumulated distance (the total distance travelled by the cell during the course of the entire microscopy recording); 4) forward migration index (FMI; the ratio between the net distance travelled along the relevant axis and the accumulated distance); 5) directness (the ratio between the Euclidian distance and the accumulated distance, denotes the tendency of the cells to migrate along a straight line); 6) velocity (36). We defined a positive chemotaxis effect if the cells migrated along the chemokine gradient (Y-axis) i.e., if the Y-COM was significantly greater than X-COM and FMI^Y was significantly greater than FMI^X.

cAMP determination

Activated $CD8^+$ T cells were lysed using 0.1M HCl at a final concentration of $1{\times}10^6$ cells/ml. Intracellular cAMP concentrations were measured in T cell lysates using the acetylated procedure of the Direct cAMP ELISA kit (Enzo Life Sciences) according to the manufacturer's instructions.

PKA kinase activity assay

Activated $CD8^+$ T were stimulated with 1 μM CGS21680 for 30 minutes. Cell lysates were prepared as previously described and total protein content was measured using BCA Protein Assay (56). The cell lysates were diluted to equal protein concentrations using kinase

activity assay buffer. The PKA kinase activity was measured using a PKA kinase activity kit (Enzo Life Sciences) as described by manufacturer with a reaction time of 90 minutes at 30°C and a development time of 60 minutes. The relative kinase activity was determined by the absorbance of the sample at 450 nm divided by the amount (μg) of crude protein.

Immunohistochemistry

Slides prepared from formalin-fixed paraffin embedded (FFPE) tumor biopsy specimens from 16 HNSCC cases were deparaffinized and stained with a monoclonal rabbit anti-human CD8 antibody (Clone SP57, Ventana Medical Systems) in a Ventana BenchMark ULTRA automated IHC slide staining system (Ventana Medical Systems). For CD73 staining, FFPE sections were stained with a mouse monoclonal anti-human CD73 antibody (Clone 1D7, Abcam). UltraView Universal DAB detection kit (Ventana Medical Systems) containing a horseradish peroxide (HRP) multimer and 3,3'-diaminobenzidine tetrahydrochloride (DAB) chromogen was used for indirect detection of the primary antibody. The slides were counterstained with hematoxylin and images were obtained at 10X magnification on an Olympus BX53 light microscope (Olympus Corporation) or on a Leica DMi8 inverted microscope with Leica Application Suite X software (Leica Microsystems inc). Tumor regions in the stained slides were identified by a pathologist and at least 4–10 fields per slide were imaged. $CD8^+$ T cell infiltration in the tumor area was digitally quantitated by drawing a region of interest (ROI) around the tumor region and counting the number of cells (brown signal) within the ROI using NIS-Elements Viewer software (Nikon Instruments Inc.). Data were expressed as cells counted per mm^2 and the median value of $CD8^+$ infiltration in all of the measured ROIs was determined. Tumors with $CD8^+$ infiltration values (cells/mm^2) above and below the median were considered as "high" and "low" infiltrated, respectively. Slides stained for CD73 were visually assessed for CD73 staining (brown signal) in the tumor and stromal regions by a pathologist and characterized as having "high" or "low" CD73 staining in these regions. To eliminate a subjective bias in reporting the $CD8^+$ infiltration as well as CD73 staining, microscopy as well as the image analysis was performed blinded.

Electrophysiology

KCa3.1 and Kv1.3 currents in $CD8^+$ T cells were measured in whole-cell voltage-clamp configuration using an Axopatch 200B amplifier (Molecular Devices). The external solution contained either 160mM NaCl, 4.5mM KCl, 2.0mM $CaCl_2$, 1.0mM $MgCl_2$, and 10mM HEPES (pH 7.4) (Fig. 5A–C), or 145mM Na-aspartate, 5mM KCl, 2.5mM $CaCl_2$, 1.0mM $MgCl_2$, 5.5mM glucose and 10mM HEPES (pH 7.4) (Fig. 6A), and the pipette solution contained 145mM K-aspartate, 10mM K_2EGTA, 8.5mM $CaCl_2$, 2mM $MgCl_2$, and 10mM HEPES (pH 7.2), 290–310 mOsm (1 μM free Ca^{2+} concentration). Currents were induced by 200-ms ramp depolarization from −120 to +40 mV from a holding potential (HP) of −70 mV every 10 s. The macroscopic conductance of KCa3.1 channels ($G_{KCa3.1}$) was calculated as a ratio of the linear fraction of macroscopic current slope to the slope of ramp voltage stimulus after subtraction of the leak current: $G(pS) = \frac{\left\{Islope\left(\frac{pA}{ms}\right)\right\}}{\left\{Vslope\left(\frac{V}{ms}\right)\right\}}$. The slope conductance was measured between −100 and −80 mV to avoid contamination by the Kv1.3 current. Kv1.3

currents were determined from the same ramp protocol at +40 mV after subtraction of the KCa3.1 current extrapolated by linear regression.

Statistical Analysis

Statistical analyses were performed using Student's t-test (paired or unpaired), Mann-Whitney rank sum test, Wilcoxon signed-rank test (in experiments where samples failed normality), and ANOVA as indicated. Post-hoc testing on ANOVA was done by multiple pairwise comparison procedures using the Holm-Sidak method. Statistical analysis was performed using SigmaPlot 13.0 (Systat Software Inc.). Outliers were determined by Grubb's test (Graph pad software). P value of less than or equal to 0.05 was defined as statistically significant. The correlation between $CD8^+$ T cell infiltration and inhibition of Y-COM was analyzed by Spearman's rank-order correlation.

Supplementary Material

Refer to Web version on PubMed Central for supplementary material.

Acknowledgments

The authors would like to acknowledge clinical coordinators from the University of Cincinnati Cancer Institute's clinical trials office (UCCI CTO) for their assistance in collection of patient samples. The authors also thank Dr. Heather Duncan (Department of Internal Medicine, Division of Nephrology and Hypertension, University of Cincinnati) for her assistance with IRB regulatory affairs. The authors would like to thank Dr. Roman Jandarov (Department of Biostatistics and Bioinformatics, University of Cincinnati) for his valuable advice on statistical analysis. The authors would also like to thank the Center for Clinical and Translational Science and Training (CCTST), University of Cincinnati for providing REDCap for effective patient data management. The authors are grateful to Dr. Heike Wulff (Department of Pharmacology, University of California Davis) for her kind gift of TRAM-34. Confocal microscopy images were acquired at the Live Microscopy Core, Department of Pharmacology and Systems Physiology, University of Cincinnati. Flow cytometry experiments were performed at Shriner's Hospital for Children Flow Cytometry Core, Cincinnati OH. **Funding**: This work was funded by grant support from the NIH (grant R01CA95286), a Pilot grant from the University of Cincinnati Cancer Institute and a Just-In-Time Core Grant from Center for Clinical and Translational Science and Training, University of Cincinnati to LC. TW-D was supported by a CTSA awarded KL2 Mentored grant, a HOTSA/HOPGA pilot grant from the Division of Hematology/Oncology at the University of Cincinnati and a grant from Center for Clinical and Translational Science and Training (1UL1TR001425-01). AB was co-financed by Campus Hungary Program (B2/1SZ/12351) and National Excellence Program (TÁMOP 4.2.4. A/2-11-1-2012-0001 B). PH was supported in part by the Bolyai János Fellowship (Hungarian Academy of Sciences).

References and Notes

1. Fang J, Li X, Ma D, Liu X, Chen Y, Wang Y, Lui VWY, Xia J, Cheng B, Wang Z. Prognostic significance of tumor infiltrating immune cells in oral squamous cell carcinoma. BMC Cancer. 2017; 17:375. [PubMed: 28549420]
2. De Meulenaere A, Vermassen T, Aspeslagh S, Zwaenepoel K, Deron P, Duprez F, Rottey S, Ferdinande L. Prognostic markers in oropharyngeal squamous cell carcinoma: focus on CD70 and tumour infiltrating lymphocytes. Pathology. 2017; 49:397–404. [PubMed: 28427753]
3. Balermpas P, Rödel F, Weiss C, Rödel C, Fokas E. Tumor-infiltrating lymphocytes favor the response to chemoradiotherapy of head and neck cancer. OncoImmunology. 2014; 3:e27403. [PubMed: 24711959]
4. Kershaw MH, Westwood JA, Darcy KP. Gene-engineered T cells for cancer therapy. Nat Rev Cancer. 2013; 13:525–541. [PubMed: 23880905]
5. Beavis PA, Milenkovski N, Henderson MA, John LB, Allard B, Loi S, Kershaw MH, Stagg J, Darcy PK. Adenosine Receptor 2A Blockade Increases the Efficacy of Anti-PD-1 through Enhanced Antitumor T-cell Responses. Cancer Immunol Res. 2015; 3:506–517. [PubMed: 25672397]

6. Beavis PA, Henderson MA, Giuffrida L, Mills JK, Sek K, Cross RS, Davenport AJ, John LB, Mardiana S, Slaney CY, Johnstone RW, Trapani JA, Stagg J, Loi S, Kats L, Gyorki D, Kershaw MH, Darcy PK. Targeting the adenosine 2A receptor enhances chimeric antigen receptor T cell efficacy. The Journal of Clinical Investigation. 2017; 127:929–941. [PubMed: 28165340]
7. Restifo NP, Dudley ME, Rosenberg SA. Adoptive immunotherapy for cancer: harnessing the T cell response. Nature reviews. Immunology. 2012; 12:269–281. [PubMed: 22437939]
8. Joyce JA, Fearon DT. T cell exclusion, immune privilege, and the tumor microenvironment. Science. 2015; 348:74–80. [PubMed: 25838376]
9. Sitkovsky MV, Lukashev D, Apasov S, Kojima H, Koshiba M, Caldwell C, Ohta A, Thiel M. Physiological Control of Immune Response and Inflammatory Tissue Damage by Hypoxia-Inducible Factors and Adenosine A2A Receptors. Annual Review of Immunology. 2004; 22:657–682.
10. Sitkovsky MV, Hatfield S, Abbott R, Belikoff B, Lukashev D, Ohta A. Hostile, hypoxia-A2-adenosinergic tumor biology as the next barrier to overcome for tumor immunologists. Cancer Immunol Res. 2014; 2:598–605. [PubMed: 24990240]
11. Allard D, Turcotte M, Stagg J. Targeting A2 adenosine receptors in cancer. Immunol Cell Biol. 2017; 95:333–339. [PubMed: 28174424]
12. Stagg J, Divisekera U, Duret H, Sparwasser T, Teng MWL, Darcy PK, Smyth JM. CD73-Deficient Mice Have Increased Antitumor Immunity and Are Resistant to Experimental Metastasis. Cancer Research. 2011; 71:2892–2900. [PubMed: 21292811]
13. Allard B, Longhi MS, Robson SC, Stagg J. The ectonucleotidases CD39 and CD73: Novel checkpoint inhibitor targets. Immunological Reviews. 2017; 276:121–144. [PubMed: 28258700]
14. Loi S, Pommey S, Haibe-Kains B, Beavis PA, Darcy PK, Smyth MJ, Stagg J. CD73 promotes anthracycline resistance and poor prognosis in triple negative breast cancer. Proceedings of the National Academy of Sciences. 2013; 110:11091–11096.
15. Turcotte M, Allard D, Mittal D, Bareche Y, Buisseret L, José V, Pommey S, Delisle V, Loi S, Joensuu H, Kellokumpu-Lehtinen P-L, Sotiriou C, Smyth MJ, Stagg J. CD73 Promotes Resistance to HER2/ErbB2 Antibody Therapy. Cancer Research. 2017; 77:5652–5663. [PubMed: 28855210]
16. Ohta A, Gorelik E, Prasad SJ, Ronchese F, Lukashev D, Wong MK, Huang X, Caldwell S, Liu K, Smith P, Chen JF, Jackson EK, Apasov S, Abrams S, Sitkovsky M. A2A adenosine receptor protects tumors from antitumor T cells. Proc Natl Acad Sci U S A. 2006; 103:13132–13137. [PubMed: 16916931]
17. Hatfield SM, Kjaergaard J, Lukashev D, Schreiber TH, Belikoff B, Abbott R, Sethumadhavan S, Philbrook P, Ko K, Cannici R, Thayer M, Rodig S, Kutok JL, Jackson EK, Karger B, Podack ER, Ohta A, Sitkovsky VM. Immunological mechanisms of the antitumor effects of supplemental oxygenation. Science Translational Medicine. 2015; 7:277ra230.
18. Allard B, Pommey S, Smyth MJ, Stagg J. Targeting CD73 enhances the antitumor activity of anti-PD-1 and anti-CTLA-4 mAbs. Clin Cancer Res. 2013; 19
19. Zhang B. CD73: A Novel Target for Cancer Immunotherapy. Cancer Research. 2010; 70:6407–6411. [PubMed: 20682793]
20. Stagg J, Beavis PA, Divisekera U, Liu MCP, Möller A, Darcy PK, Smyth JM. CD73-Deficient Mice Are Resistant to Carcinogenesis. Cancer Research. 2012; 72:2190–2196. [PubMed: 22396496]
21. Pardoll DM. The blockade of immune checkpoints in cancer immunotherapy. Nat Rev Cancer. 2012; 12:252–264. [PubMed: 22437870]
22. Chimote AA, Hajdu P, Kucher V, Boiko N, Kuras Z, Szilagyi O, Yun YH, Conforti L. Selective inhibition of KCa3.1 channels mediates adenosine regulation of the motility of human T cells. Journal of immunology. 2013; 191:6273–6280.
23. Cahalan MD, Chandy KG. The functional network of ion channels in T lymphocytes. Immunol Rev. 2009; 231:59–87. [PubMed: 19754890]
24. Kuras Z, Yun YH, Chimote AA, Neumeier L, Conforti L. KCa3.1 and TRPM7 channels at the uropod regulate migration of activated human T cells. PLoS One. 2012; 7:e43859. [PubMed: 22952790]

25. Hu L, Wang T, Gocke AR, Nath A, Zhang H, Margolick JB, Whartenby KA, Calabresi PA. Blockade of Kv1.3 Potassium Channels Inhibits Differentiation and Granzyme B Secretion of Human CD8+ T Effector Memory Lymphocytes. PLoS ONE. 2013; 8:e54267. [PubMed: 23382885]
26. Feske S, Skolnik EY, Prakriya M. Ion channels transporters in lymphocyte function, immunity. Nature reviews. Immunology. 2012; 12:532–547. [PubMed: 22699833]
27. Conforti L, Petrovic M, Mohammad D, Lee S, Ma Q, Barone S, Filipovich AH. Hypoxia regulates expression and activity of Kv1.3 channels in T lymphocytes: a possible role in T cell proliferation. J Immunol. 2003; 170:695–702. [PubMed: 12517930]
28. Robbins JR, Lee SM, Filipovich AH, Szigligeti P, Neumeier L, Petrovic M, Conforti L. Hypoxia modulates early events in T cell receptor-mediated activation in human T lymphocytes via Kv1.3 channels. The Journal of Physiology. 2005; 564:131–143. [PubMed: 15677684]
29. Szigligeti P, Neumeier L, Duke E, Chougnet C, Takimoto K, Lee SM, Filipovich AH, Conforti L. Signalling during hypoxia in human T lymphocytes - critical role of the src protein tyrosine kinase p56Lck in the O2 sensitivity of Kv1.3 channels. J Physiol. 2006; 573:357–370. [PubMed: 16600997]
30. Chimote AA, Hajdu P, Sfyris AM, Gleich BN, Wise-Draper T, Casper KA, Conforti L. Kv1.3 Channels Mark Functionally Competent CD8+Tumor-Infiltrating Lymphocytes in Head and Neck Cancer. Cancer Research. 2017; 77:53–61. [PubMed: 27815390]
31. Eil R, Vodnala SK, Clever D, Klebanoff CA, Sukumar M, Pan JH, Palmer DC, Gros A, Yamamoto TN, Patel SJ, Guittard GC, Yu Z, Carbonaro V, Okkenhaug K, Schrump DS, Linehan WM, Roychoudhuri R, Restifo NP. Ionic immune suppression within the tumour microenvironment limits T cell effector function. Nature. 2016; 537:539–543. [PubMed: 27626381]
32. Gurusamy D, Clever D, Eil R, Restifo NP. Novel “Elements” of Immune Suppression within the Tumor Microenvironment. Cancer Immunology Research. 2017; 5:426–433. [PubMed: 28576921]
33. Mandapathil M, Szczepanski M, Harasymczuk M, Ren J, Cheng D, Jackson EK, Gorelik E, Johnson J, Lang S, Whiteside TL. CD26 expression and adenosine deaminase activity in regulatory T cells (Treg) and CD4(+) T effector cells in patients with head and neck squamous cell carcinoma. Oncoimmunology. 2012; 1:659–669. [PubMed: 22934258]
34. Young A, Mittal D, Stagg J, Smyth MJ. Targeting cancer-derived adenosine: new therapeutic approaches. Cancer Discov. 2014; 4:879–888. [PubMed: 25035124]
35. Hara-Chikuma M, Chikuma S, Sugiyama Y, Kabashima K, Verkman AS, Inoue S, Miyachi Y. Chemokine-dependent T cell migration requires aquaporin-3-mediated hydrogen peroxide uptake. J Exp Med. 2012; 209:1743–1752. [PubMed: 22927550]
36. Zengel P, Nguyen-Hoang A, Schildhammer C, Zantl R, Kahl V, Horn E. μ-Slide Chemotaxis: A new chamber for long-term chemotaxis studies. BMC Cell Biology. 2011; 12:21. [PubMed: 21592329]
37. Albert S, Riveiro ME, Halimi C, Hourseau M, Couvelard A, Serova M, Barry B, Raymond E, Faivre S. Focus on the role of the CXCL12/CXCR4 chemokine axis in head and neck squamous cell carcinoma. Head & Neck. 2013; 35:1819–1828. [PubMed: 23468253]
38. Csoka B, Himer L, Selmeczy Z, Vizi ES, Pacher P, Ledent C, Deitch EA, Spolarics Z, Nemeth ZH, Hasko G. Adenosine A2A receptor activation inhibits T helper 1 and T helper 2 cell development and effector function. Faseb J. 2008; 22:3491–3499. [PubMed: 18625677]
39. Wulff H, Miller MJ, Hansel W, Grissmer S, Cahalan MD, Chandy KG. Design of a potent and selective inhibitor of the intermediate-conductance Ca2+-activated K+ channel, IKCa1: a potential immunosuppressant. Proc Natl Acad Sci U S A. 2000; 97:8151–8156. [PubMed: 10884437]
40. Ghanshani S, Wulff H, Miller MJ, Rohm H, Neben A, Gutman GA, Cahalan MD, Chandy KG. Up-regulation of the IKCa1 potassium channel during T-cell activation. Molecular mechanism and functional consequences. J Biol Chem. 2000; 275:37137–37149. [PubMed: 10961988]
41. Cui M, Qin G, Yu K, Bowers MS, Zhang M. Targeting the Small- and Intermediate-Conductance Ca²⁺-Activated Potassium Channels: The Drug-Binding Pocket at the Channel/Calmodulin Interface. Neurosignals. 2014; 22:65–78. [PubMed: 25300231]

42. Coleman N, Brown BM, Oliván-Viguera A, Singh V, Olmstead MM, Valero MS, Köhler R, Wulff H. New Positive Ca2+-Activated K+ Channel Gating Modulators with Selectivity for KCa3.1. Molecular Pharmacology. 2014; 86:342–357. [PubMed: 24958817]
43. Chen DS, Mellman I. Elements of cancer immunity and the cancer-immune set point. Nature. 2017; 541:321–330. [PubMed: 28102259]
44. Mellman I, Coukos G, Dranoff G. Cancer immunotherapy comes of age. Nature. 2011; 480:480–489. [PubMed: 22193102]
45. Alhamarneh O, Amarnath SMP, Stafford ND, Greenman J. Regulatory T cells: What role do they play in antitumor immunity in patients with head and neck cancer? Head & Neck. 2008; 30:251–261. [PubMed: 18172882]
46. Antonioli L, Yegutkin GG, Pacher P, Blandizzi C, Haskó G. Anti-CD73 in Cancer Immunotherapy: Awakening New Opportunities. Trends in Cancer. 2016; 2:95–109. [PubMed: 27014745]
47. Häusler SFM, Montalbán del Barrio I, Strohschein J, Anoop Chandran P, Engel JB, Hönig A, Ossadnik M, Horn E, Fischer B, Krockenberger M, Heuer S, Seida AA, Junker M, Kneitz H, Kloor D, Klotz K-N, Dietl J, Wischhusen J. Ectonucleotidases CD39 and CD73 on OvCA cells are potent adenosine-generating enzymes responsible for adenosine receptor 2A–dependent suppression of T cell function and NK cell cytotoxicity. Cancer Immunology, Immunotherapy. 2011; 60:1405. [PubMed: 21638125]
48. Turcotte M, Spring K, Pommey S, Chouinard G, Cousineau I, George J, Chen GM, Gendoo DMA, Haibe-Kains B, Karn T, Rahimi K, Le Page C, Provencher D, Mes-Masson A-M, Stagg J. CD73 Is Associated with Poor Prognosis in High-Grade Serous Ovarian Cancer. Cancer Research. 2015; 75:4494–4503. [PubMed: 26363007]
49. Leclerc BG, Charlebois R, Chouinard G, Allard B, Pommey S, Saad F, Stagg J. CD73 Expression Is an Independent Prognostic Factor in Prostate Cancer. Clinical Cancer Research. 2016; 22:158–166. [PubMed: 26253870]
50. Ma S-R, Deng W-W, Liu J-F, Mao L, Yu G-T, Bu L-L, Kulkarni AB, Zhang W-F, Sun Z-J. Blockade of adenosine A2A receptor enhances CD8+ T cells response and decreases regulatory T cells in head and neck squamous cell carcinoma. Molecular Cancer. 2017; 16:99. [PubMed: 28592285]
51. Cronstein BN, Sitkovsky M. Adenosine and adenosine receptors in the pathogenesis and treatment of rheumatic diseases. Nat Rev Rheumatol. 2017; 13:41–51. [PubMed: 27829671]
52. Eltzschig HK, Sitkovsky MV, C S. Robson Purinergic Signaling during Inflammation. New England Journal of Medicine. 2012; 367:2322–2333. [PubMed: 23234515]
53. Ohta A, Gorelik E, Prasad SJ, Ronchese F, Lukashev D, Wong MK, Huang X, Caldwell S, Liu K, Smith P, Chen JF, Jackson EK, Apasov S, Abrams S, Sitkovsky M. A2A adenosine receptor protects tumors from antitumor T cells. Proc Natl Acad Sci U S A. 2006; 103:13132–13137. [PubMed: 16916931]
54. Mandapathil M, Szczepanski MJ, Szajnik M, Ren J, Jackson EK, Johnson JT, Gorelik E, Lang S, Whiteside TL. Adenosine and Prostaglandin E2 Cooperate in the Suppression of Immune Responses Mediated by Adaptive Regulatory T Cells. Journal of Biological Chemistry. 2010; 285:27571–27580. [PubMed: 20558731]
55. Chimote AA, Hajdu P, Kottyan LC, Harley JB, Yun Y, Conforti L. Nanovesicle-targeted Kv1.3 knockdown in memory T cells suppresses CD40L expression and memory phenotype. J Autoimmun. 2016; 69:86–93. [PubMed: 26994905]
56. Chimote AA, Kuras Z, Conforti L. Disruption of kv1.3 channel forward vesicular trafficking by hypoxia in human T lymphocytes. The Journal of biological chemistry. 2012; 287:2055–2067. [PubMed: 22134923]

Editor's summary

Reduced K^+ channel activity curbs T cell migration

T cell accumulation in solid tumors is limited by multiple factors found within the tumor microenvironment, including the nucleoside adenosine. Chimote *et al.* analyzed the migration of $CD8^+$ T cells in a 3D chemotaxis assay and found that adenosine inhibited the chemotaxis of T cells from cancer patients more than T cells from healthy donors. The increased sensitivity of patient $CD8^+$ T cells to adenosine correlated with reduced KCa3.1 potassium channel activity, but not adenosine receptor expression or signaling. Treatment with a KCa3.1 channel agonist restored patient $CD8^+$ T cell migration in the presence of adenosine, suggesting that K^+ channel activators may help augment T cell infiltration of adenosine-rich solid tumors.

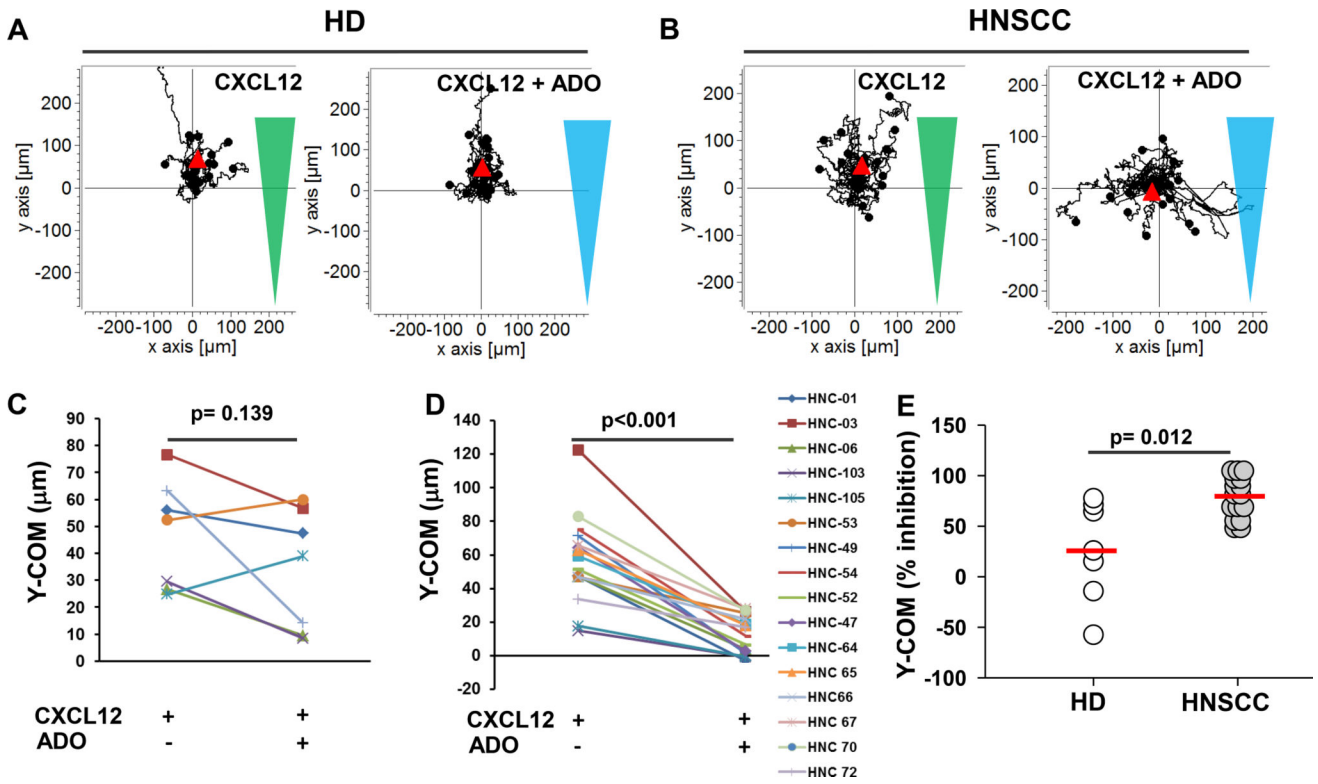

Fig. 1. HNSCC CD8$^+$ T cells exhibit reduced chemotaxis in the presence of adenosine

(**A** and **B**) Trajectories of CD8$^+$ T cells migrating along either a CXCL12 gradient (green triangles) or a combination gradient of CXCL12 with adenosine (ADO, blue triangles) in a representative HD (A) and HNSCC patient (B). Trajectories of at least 15–20 cells are shown for each condition and the starting point of each cell trajectory is artificially set to the same origin. The red triangles represent Y-COM. (C and D) Y-COM values for cells migrating along either a CXCL12 gradient or a combination gradient of CXCL12 with adenosine in HDs (C; n=7 donors) and HNSCC patients (D; n=16 patients). (E) Percentage inhibition in the Y-COM values in the presence of CXCL12 and adenosine (values shown in C and D) in HD (n=7 donors) and HNSCC (n=16 patients). Horizontal red line represents mean values for each group. Data in C and D were analyzed by paired Student's t-test and in panel E by Mann-Whitney rank sum test.

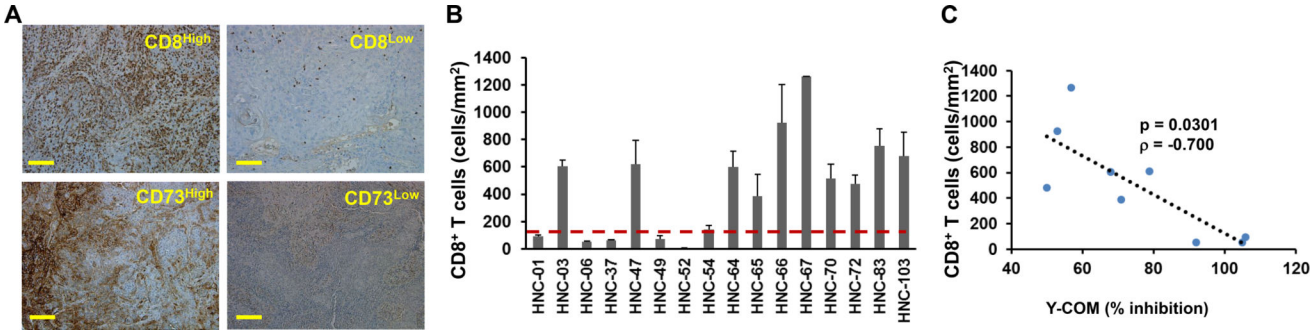

Fig. 2. Tumor infiltration is dependent on the sensitivity of circulating CD8$^+$ T cells to adenosine

(A) Immunohistochemistry of CD8 (top) and CD73 (bottom) expression (brown signal) in representative HNSCC tumor tissues showing low and high infiltration by CD8$^+$ T cells and low and high CD73 expression (Table S1). Scale bar = 100 μm. (B) Bar graph showing the number of CD8$^+$ T cells (cells/mm^2) within the tumor region in 16 HNSCC tumors. Please note that donor HNC-52 has a mean CD8$^+$ T cell infiltration value of 5 cells/mm^2. The broken red line represents the median value for the 16 HNSCC patients. The tumors with CD8$^+$ T cell infiltration above the median value were considered to be "well-infiltrated" (Referred as "High" in Table S1), whereas the tumors with CD8$^+$ T cell infiltration below the median value were considered to be "poorly-infiltrated" (Referred as "Low" in Table S1). The bars represent mean ± SEM. (C) Correlation between CD8$^+$ T cell infiltration and percentage reduction of the Y-COM values in the presence of CXCL12 and adenosine (values shown in Fig. 1E) in 9 HNSCC patients that were scored as CD73^{high} (see Table S1). Correlation was measured by Spearman rank order correlation test ($p = 0.0301$, correlation coefficient, $\rho = -0.700$).

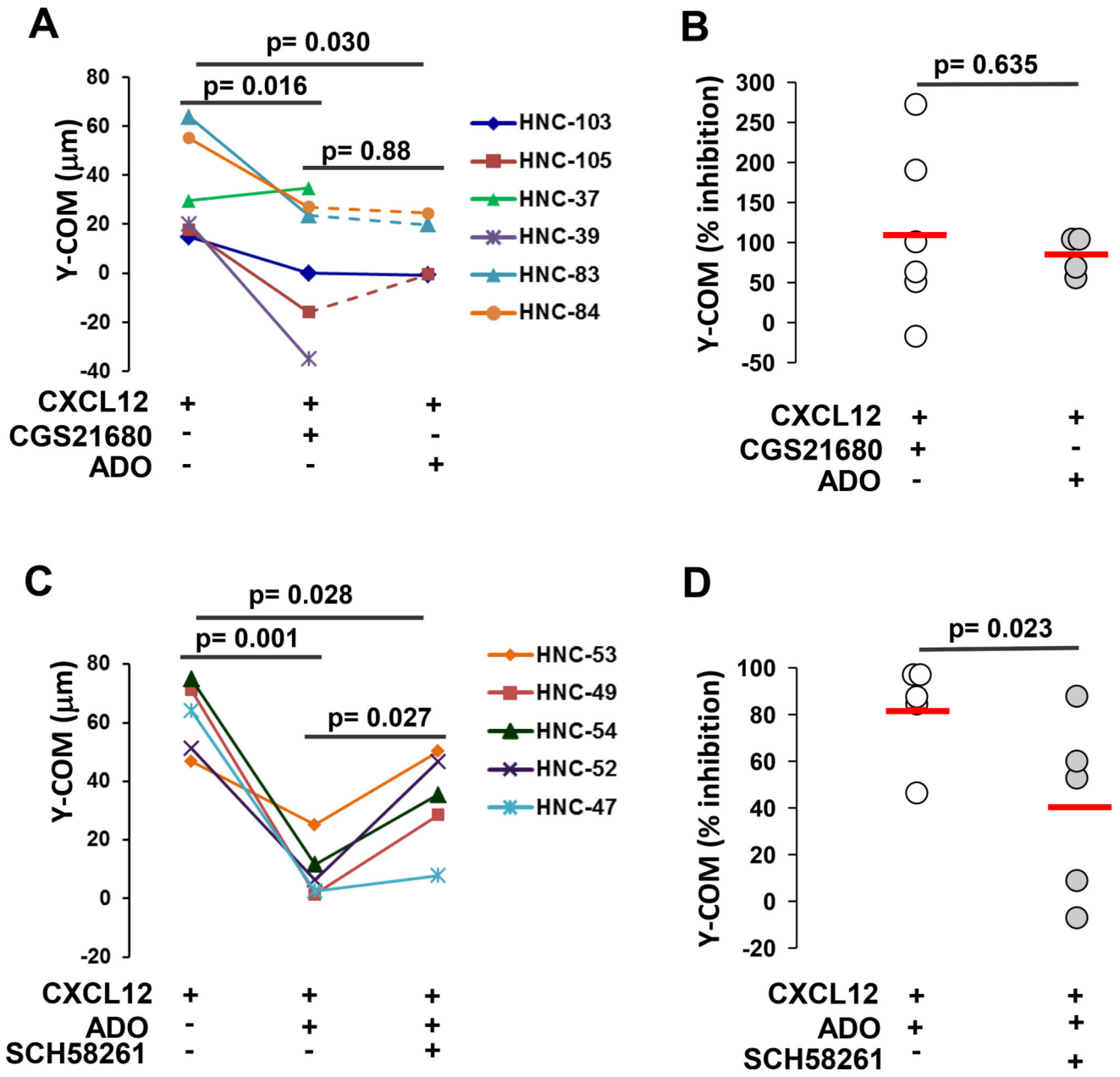

Fig. 3. $A_{2A}R$ mediates the suppressive effect of adenosine on the chemotaxis of HNSCC $CD8^+$ T cells

(A) Y-COM values for HNSCC $CD8^+$ T cells migrating along either a CXCL12 gradient (n=6 patients), a combination gradient of CXCL12 with CGS21680 (n=6 patients), or CXCL12 with adenosine (ADO, n=4 patients). (B) Percentage inhibition in the Y-COM values for each individual experiment shown in (A) after incubation with CGS21680 or adenosine. Horizontal red lines represent mean values for each group. (C) Y-COM values for HNSCC $CD8^+$ T cells pretreated with or without 1 µM SCH58261 migrating toward CXCL12 in the presence of adenosine. Untreated $CD8^+$ T cells in a CXCL12 gradient were used as controls (n=5 patients). (D) Percentage inhibition in the Y-COM values by adenosine for each of the donors shown in (C) with or without SCH58261 pretreatment. Horizontal red

line represents mean values for each group. Data in A and C were analyzed by one-way repeated measures ANOVA (p=0.010 for A, and p=0.001 for C); in B and D by t-test.

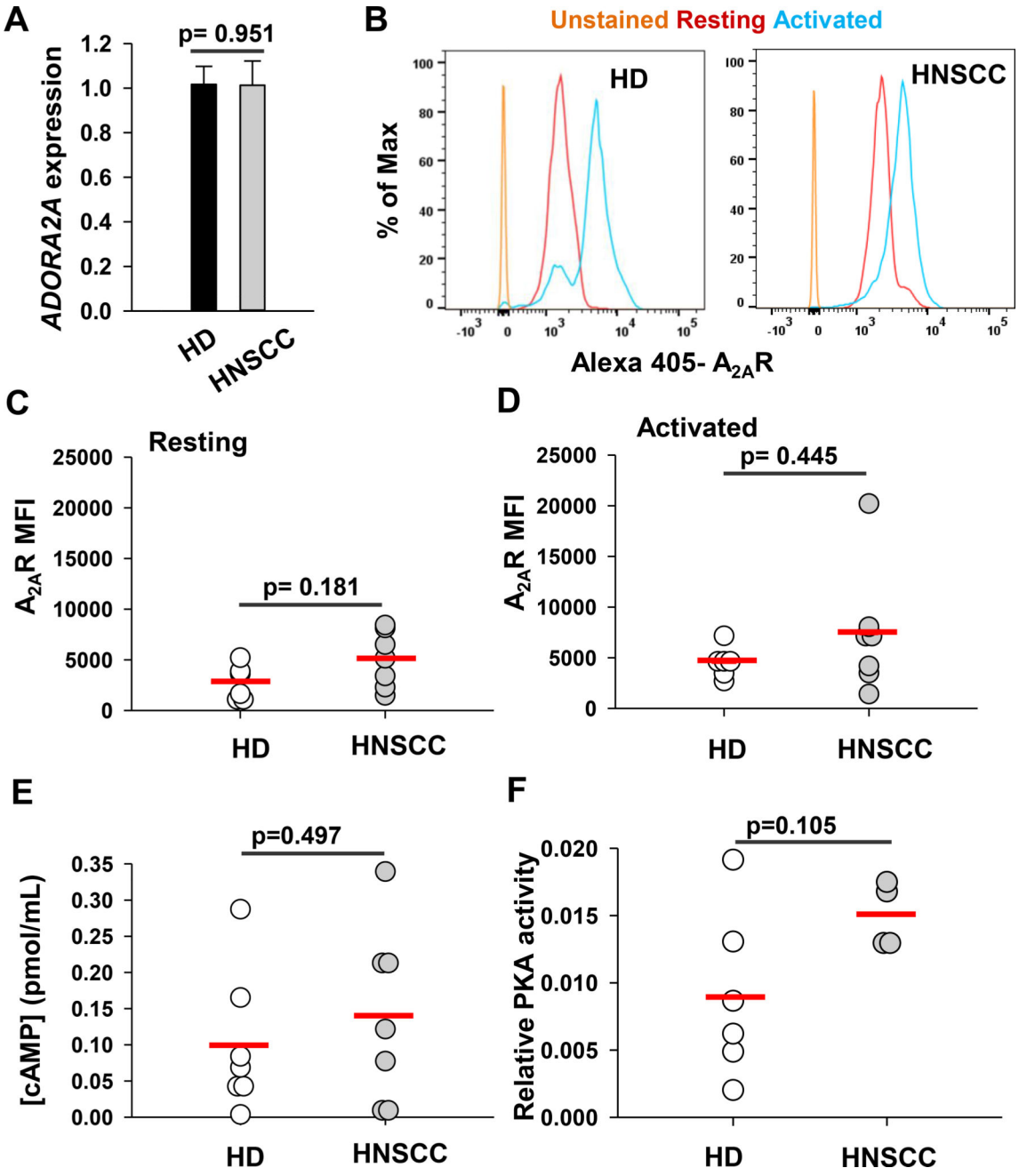

Fig. 4. $A_{2A}R$ expression and $A_{2A}R$ signaling are not altered in HNSCC $CD8^+$ T cells

(A) *ADORA2A* expression in activated HD and HNSCC $CD8^+$ T cells was quantified by RT-qPCR. Data are the fold-change in *ADORA2A* expression relative to *GAPDH* expression. The data were normalized to the mean *ADORA2A* expression in HD. Data are mean ± SEM for from 4 HD and 5 HNSCC patients. (B) Representative flow cytometry histograms showing $A_{2A}R$ expression in resting and activated $CD8^+$ T cells from HD and HNSCC. (C–D) Mean fluorescence intensity (MFI) of $A_{2A}R$ measured in resting (C) and activated (D) $CD8^+$ T cells from HD (n=6 donors) and HNSCC patients (n=7 patients). (E) cAMP concentration in $CD8^+$ T cells from HD (n=7 donors) and HNSCC patients (n=7

patients). (F) Relative PKA activity in $CD8^+$ T cells from HD (n=3 donors) and HNSCC patients (n=4 patients). Horizontal red line represents mean values for each group. Data in C, D and F were analyzed by Mann-Whitney rank sum test; data in A and E were analyzed by t-test.

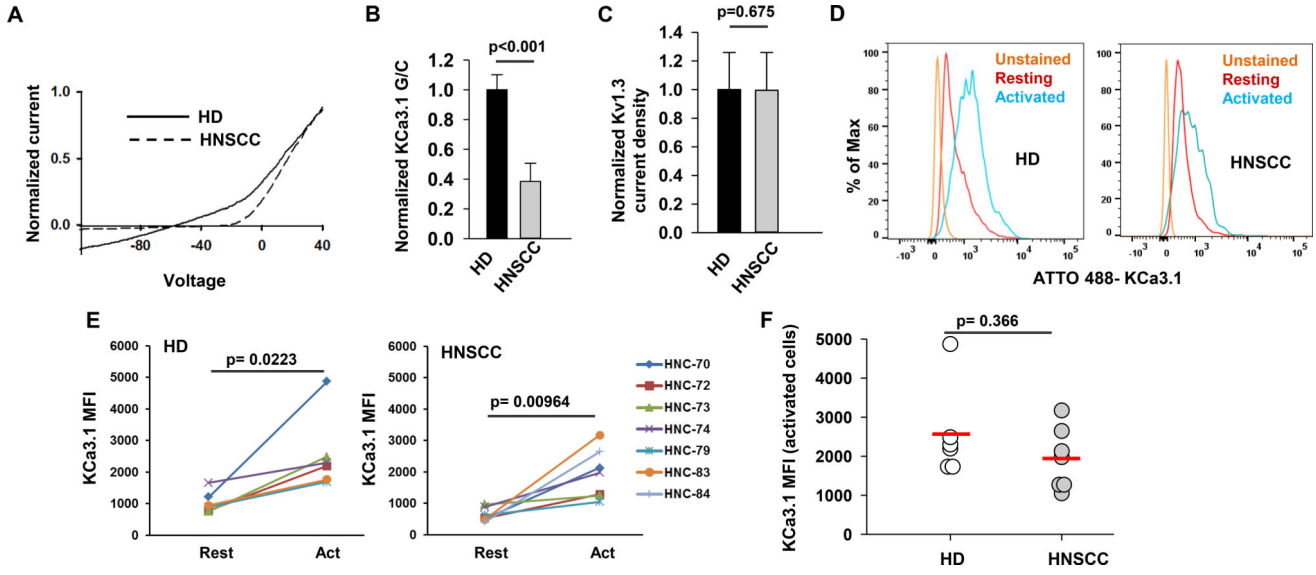

Fig. 5. KCa3.1 channel activity is reduced in HNSCC CD8$^+$ T cells

(A) Representative KCa3.1 currents in CD8$^+$ T cells recorded in whole-cell voltage clamp configuration from a HD and HNSCC patient. Currents were normalized for the maximum current at +40 mV to ease comparison of the KCa3.1 conductance at hyperpolarizing voltages. (B) KCa3.1 conductance (normalized to cell capacitance, G/C) measured in activated CD8$^+$ T cells from HD (n=30 cells, 6 donors) and HNSCC patients (n= 21 cells, 4 patients). (C) Kv1.3 channel current density measured in activated CD8$^+$ T cells from HD (n=25 cells, 5 donors) and HNSCC patients (n= 21 cells, 4 patients). For B and C, the data are normalized to values measured in activated CD8$^+$ T cells from HD and the bars represent mean ± SEM. (D) Representative flow cytometry histograms showing KCa3.1 expression in resting and activated CD8$^+$ T cells from HD and HNSCC patients. (E) Mean fluorescence intensity (MFI) of KCa3.1 measured in resting and activated CD8$^+$ T cells from HD (n=6 donors) and HNSCC patients (n=7 patients). (F) KCa3.1 MFI in activated CD8$^+$ T cells from HD (n=6 donors) and HNSCC (n= 7 patients). Horizontal red line represents mean values for each group. Data in B, C and F were analyzed by Mann-Whitney rank sum test; E by paired t-test.

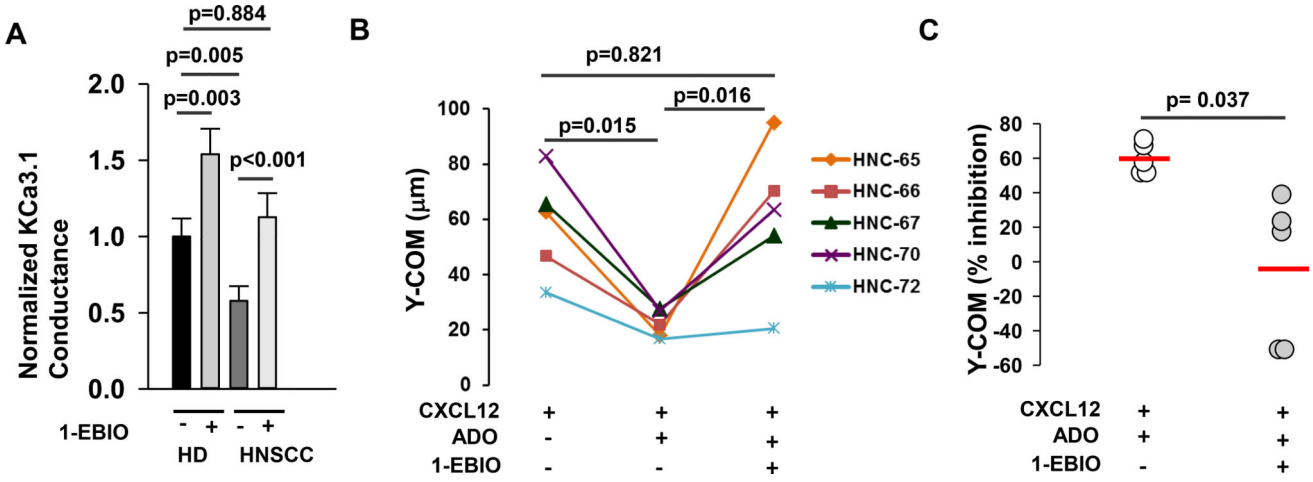

Fig. 6. Activation of KCa3.1 channels restores the chemotaxis of HNSCC CD8$^+$ T cells in the presence of adenosine

(A) KCa3.1 channel conductance in the presence or absence of 100 μM 1-EBIO was measured in activated CD8$^+$ T cells from HD (n=17 cells, 4 donors) and HNSCC patients (n= 24 cells, 5 patients). The data were normalized to untreated (no 1-EBIO) activated cells from HD. The data are mean ± SEM. (B) Y-COM values calculated for HNSCC CD8$^+$ T cells migrating along either a CXCL12 gradient or a combination gradient of CXCL12 with adenosine with or without preincubation with 20 μM 1-EBIO (n=5 patients). (C) Percentage inhibition in the Y-COM values (B) of the cells pretreated with 1-EBIO. Horizontal red line represents mean values for each group. Data in A were analyzed by two-way ANOVA; whereas data in B were analyzed with one-way repeated measures ANOVA (p=0.009) and C with paired t-test.

Table 1
Demographics of HNSCC patients enrolled in the study

Patients matching the inclusion criteria (n=39) were enrolled in the study. ECOG performance status describes how the disease affects the daily living abilities of the patient. For evaluating smoking status, pack years are calculated by multiplying the number of packs of cigarettes smoked per day by the number of years the person has smoked. Tumor stage from T1 to T4 refers to the size and extent of the tumors. The involvement of regional lymph nodes is referred by N1 to N3 depending on the number and location of the lymph nodes involved. N0 denotes absence of cancer in the regional lymph nodes.

Age (at the time of sample collection)	**Years**
Range	34 to 77
Mean	56
Variable	**Number (%)**
Gender	
Male	31 (79)
Female	8 (21)
Site	
Oral Cavity	12 (31)
Oropharynx	17 (44)
Larynx	8 (21)
Hypopharynx	1 (2)
Nasopharynx	1 (2)
Tumor stage	
T1	7 (18)
T2	10 (26)
T3	9 (23)
T4	11 (28)
Unknown	2 (5)
Nodal Status	
N0	8 (20)
N1	4 (10)
N2	24 (62)
N3	1 (3)
Unknown	2 (5)
ECOG (Eastern Cooperative Oncology Group) performance status	
0	25 (64)
1	9 (23)
2	3 (8)
Unknown	2 (5)
Smoking	
No (<10 pk years)	15 (38)

Age (at the time of sample collection)	Years
Yes (>10 pk years)	24 (62)
Alcohol	
No	28 (72)
Yes (>5 drinks/week)	11 (28)
p16 status	
Positive	16 (41)
Negative	13 (33)
Unknown	10 (26)

Table 2

Effect of adenosine on the chemotaxis of HD and HNSCC CD8$^+$ T cells

Activated CD8$^+$ T cells from HD and HNSCC patients were exposed to a gradient of either CXCL12 or CXCL12 and adenosine (ADO), and the indicated values were measured. Results are presented as mean ± SEM for all measured values.

Parameter	CXCL12	CXCL12 + ADO	p-value (CXCL12 vs CXCL12+ ADO)
HD (n= 5)			
X-COM (μm)	5.660 ± 4.739	1.586 ± 5.282	0.610
Y-COM (μm)	43.279 ± 9.221[a]	33.366 ± 10.424[b]	0.134
FMI^x	0.016 ± 0.019	−0.001 ± 0.015	0.523
FMI^y	0.141 ± 0.031[c]	0.109 ± 0.029[d]	0.001
Directness	0.203 ± 0.024	0.202 ± 0.017	0.925
Velocity (μm/s)	0.210 ± 0.021	0.182 ± 0.021	0.478
Accumulated distance (μm)	315.462 ± 31.352	272.336 ± 30.909	0.475
Euclidean distance (μm)	62.122 ± 6.277	56.081 ± 10.104	0.526
HNSCC (n=6)			
X-COM (μm)	−7.125 ± 9.596	3.943 ± 11.983	0.629
Y-COM (μm)	46.773 ± 18.178[e,i]	4.281 ± 4.829[f]	0.029
FMI^x	−0.030 ± 0.023	0.024 ± 0.036	0.404
FMI^y	0.191 ± 0.039[g]	0.005 ± 0.020[h]	<0.001
Directness	0.256 ± 0.040	0.188 ± 0.017	0.080
Velocity (μm/s)	0.146 ± 0.042	0.139 ± 0.040	0.495
Accumulated distance (μm)	211.297 ± 62.163	206.839 ± 59.620	0.725
Euclidean distance (μm)	38.126 ± 8.524	38.145 ± 10.953	0.438[i]

In HD:

[a] p = 0.002 vs X-COM

[b] p = 0.0876 vs X-COM

[c] p = 0.008 vs FMI^X

[d] p = 0.046 vs FMI^X.

In HNSCC:

[e] p = 0.031 vs X-COM

[f] p = 0.970 vs X-COM

[g] p = 0.011 vs FMI^X

[h] p = 0.610 vs FMI^X, statistical significance in

[i]measured by Wilcoxon signed-rank test, all other p-values measured by paired Student's t-test. Y-COM = center of mass along the Y-axis, along the chemokine gradient; X-COM = center of mass along the X-axis, perpendicular to the chemokine gradient; FMI^{Y} = forward migration index in the direction of the y-axis (it represents the efficiency of forward migration towards the chemokine gradient); FMI^{X} = forward migration index in the direction of the x-axis (represents the efficiency of migration perpendicular to the chemokine gradient respectively);